Limnol. Oceanogr., 57(3), 2012, 851–867

doi:10.4319/lo.2012.57.3.0851

Benthic iron and phosphorus fluxes across the Peruvian oxygen minimum zone

A. Noffke,[a,*] C. Hensen,[a] S. Sommer,[a] F. Scholz,[a] L. Bohlen,[a] T. Mosch,[a] M. Graco,[b] and K. Wallmann [a]

[a] Helmholtz-Zentrum für Ozeanforschung Kiel, Kiel, Germany
[b] Instituto del Mar del Perú, Callao, Peru

Abstract

Benthic fluxes of dissolved ferrous iron (Fe^{2+}) and phosphate (TPO_4) were quantified by in situ benthic chamber incubations and pore-water profiles along a depth transect (11°S, 80–1000 m) across the Peruvian oxygen minimum zone (OMZ). Bottom-water O_2 levels were < 2 μmol L^{-1} down to 500-m water depth, and increased to $\sim$ 40 μmol L^{-1} at 1000 m. Fe^{2+} fluxes were highest on the shallow shelf (maximum 316 mmol m^{-2} yr^{-1}), moderate (15.4 mmol m^{-2} yr^{-1}) between 250 m and 600 m, and negligible at deeper stations. In the persistent OMZ core, continuous reduction of Fe oxyhydroxides results in depletion of sedimentary Fe : Al ratios. TPO_4 fluxes were high (maximum 292 mmol m^{-2} yr^{-1}) throughout the shelf and the OMZ core in association with high organic carbon degradation rates. Ratios between organic carbon degradation and TPO_4 flux indicate excess release of P over C when compared to Redfield stoichiometry. Most likely, this is caused by preferential P release from organic matter, dissolution of fish debris, and/or P release from microbial mat communities, while Fe oxyhydroxides can only be inferred as a major P source on the shallow shelf. The benthic fluxes presented here are among the highest reported from similar, oxygen-depleted environments and highlight the importance of sediments underlying anoxic water bodies as nutrient sources to the ocean. The shelf is particularly important as the periodic passage of coastal trapped waves and associated bottom-water oxygenation events can be expected to induce a transient biogeochemical environment with highly variable release of Fe^{2+} and TPO_4.

Oxygen minimum zones (OMZ), water layers with oxygen concentrations < 20 μmol L^{-1}, are persistent hydrographic features in large parts of the ocean, in particular the eastern Pacific, the northern Indian Ocean, and the eastern Atlantic off southwest Africa (Helly and Levin 2004). One of the most extended and intense OMZs (dropping to oxygen concentrations close to anoxia in core regions; Stramma et al. 2008) is located in the eastern South Pacific, underneath the productive coastal waters of the Humboldt Current System. This OMZ stretches from 37°S, Chile, to the equatorial belt (0–5°S) and reaches its greatest extension off Peru between 5 and 13°S, with $>$ 600-m thickness to about 1000 km offshore (Fuenzalida et al. 2009).

The complex maintenance mechanisms and dynamics of OMZs still have not been sufficiently resolved. However, the principal factors leading to their formation are intense oxygen consumption in response to high surface productivity, sustained by high amounts of upwelled nutrients, and sluggish ventilation due to the hydrographic regime (Wyrtki 1962). Climate models predict an overall decline of dissolved oxygen in the ocean interior to emerge from global warming (Matear and Hirst 2003). For the tropical OMZs this decline was recently confirmed by 50-yr time series analyses of O_2 data (collected since 1960; Stramma et al. 2008).

In response to the expansion of the hypoxic water masses, major changes in nutrient cycling could occur and affect the marine carbon, nitrogen, phosphorus, and iron cycles via various feedback mechanisms. Thus, improving current knowledge on the key biogeochemical and physical processes governing today's OMZs by quantitative approaches remains critical to estimating the ocean's responses to global warming and becomes a future research challenge.

Oxygen depletion substantially affects the biogeochemical reactions of redox-sensitive elements. This in particular applies to iron (Fe) and phosphorus (P), whose individual cycles are strongly linked in the marine environment. A number of previous studies have resulted in the observation that under oxygen-deficient bottom-water conditions dissolved ferrous iron (Fe^{2+}) and phosphate (TPO_4) are preferentially released into the pore fluids and overlying bottom water (Sundby et al. 1986; Ingall and Jahnke 1997; McManus et al. 1997). Particulate ferric iron oxides and hydroxides (hereafter referred to as iron oxyhydroxides) scavenge phosphate, and oxygen deficiency promotes their reduction to soluble states by microbial induced dissolution and the concomitant liberation of metal-oxide-bound phosphate (Sundby et al. 1992). Phosphate release from iron oxyhydroxides may further be enhanced through reductive dissolution by hydrogen sulfide (Jensen et al. 1995). Furthermore, in addition to these metal oxide interactions, growing evidence has been presented that phosphate is preferentially regenerated from P-bearing organic matter (as compared to C) under hypoxic and anoxic bottom-water conditions (Ingall et al. 1993).

Despite the obvious biogeochemical significance of organic rich sediments underlying productive upwelling systems for global element cycles and related feedbacks on ocean–climate interactions, relatively few systematic in situ studies on benthic nutrient turnover have been conducted to date. Phosphate fluxes derived from benthic chamber incubations are available for the continental margins off Washington State (Devol and Christensen 1993; Hartnett and Devol 2003), central California (Ingall and Jahnke

* Corresponding author: anoffke@geomar.de

1997; McManus et al. 1997; Berelson et al. 2003), and northwest Mexico (Hartnett and Devol 2003), as well as the California borderland basins (Ingall and Jahnke 1997; McManus et al. 1997; Hammond et al. 2004). Measurements in the Arabian Sea (Woulds et al. 2009) have recently complemented the existing data pool. With regard to iron, the knowledge on benthic release rates is even smaller. This can mainly be ascribed to the fact that generally aeolian dust deposition (Jickells et al. 2005) has been assumed to be the major supply pathway of iron to the open ocean, and it was only recently that the potential contribution of a sedimentary iron source has begun to be considered (Moore and Braucher 2008). Much of the work done in continental margin upwelling settings focused on iron inventories and turnover in the water column. However, a number of these studies highlight the role of sediments supplying iron to the water column by mechanisms of resuspension (Hutchins et al. 1998) and reductive mobilization (Johnson et al. 1999). Direct measurements with benthic chambers revealed that reductive mobilization can be significant in such sedimentary settings (McManus et al. 1997; Elrod et al. 2004; Severmann et al. 2010).

In this paper we report seabed fluxes of dissolved phosphate and iron for the OMZ off Peru. To our knowledge, this represents the first detailed investigation on benthic release of this redox-sensitive couple in the eastern South Pacific upwelling region. Benthic fluxes were derived from time series of in situ incubations with benthic landers and calculations from pore-water gradients. Sampling was conducted along a latitudinal transect (11°S) at water depths from 80 m to 1000 m, affected by regionally varying environmental influences (redox conditions, hydrodynamics and organic carbon availability). This enabled us to directly link magnitudes of nutrient release with potential controlling parameters.

Methods

Regional setting—The Peruvian coast is part of the most productive marine ecosystem in the world. High primary productivity of up to 3.6 g C m^{-2} d^{-1} (Pennington et al. 2006) is sustained by coastal upwelling that transports cold, oxygen-poor but nutrient-rich water to the well-mixed surface layer. Upwelling off Peru is perennial, favored by almost constant alongshore-oriented winds, which drive an offshore Ekman transport of surface waters (Strub et al. 1998). Upwelled waters are predominantly fed by Equatorial Subsurface Water, which is transported poleward with the Peru Chile Undercurrent (Strub et al. 1998). Intensity of the coastal upwelling changes seasonally due to varying wind strength with maximum wind speed and coastal upwelling occurring in austral winter and spring (Pennington et al. 2006). The OMZ that develops from intense degradation of organic matter and associated oxygen consumption extends roughly from $<$ 100 m to 700 m (oxycline of 22 μmol L^{-1} defined by Fuenzalida et al. 2009). Seasonal changes in upwelling intensity typically result in variable mixed surface layer depths of 10 m to 40 m (Bakun 1985). However, periodic oxygenation events of the bottom waters may reach down to about 100-m water depth as observed off Callao at 12°S (Gutiérrez et al. 2008). According to this study, the vertical position of the upper boundary of the OMZ (defined as the 22 μmol L^{-1} isopleth) fluctuated between 10-m to 90-m water depth (mean depth: 52 m) over a period of 13 yr (1992–2005). Such oxygenation events are strongly associated with the passage of coastal trapped waves that occur more frequently during positive El Niño Southern Oscillation (ENSO) periods (Gutiérrez et al. 2008) and are associated with a significant deepening of the thermo- and oxycline. Most intense oxygenation events have been reported for the strong El Niño periods in 1982–1983 and 1997–1998 during which the upper boundary of the OMZ deepened to almost 300 m (Levin et al. 2002; Fuenzalida et al. 2009).

Between 11–15°S, underneath the region of most intense primary productivity (Pennington et al. 2006), organic rich ($\gg$ 5 wt%), diatomaceous muds accumulate at water depths between 50 m and 500 m (Suess et al. 1987). A distinct feature of this region is a thick lens-shaped deposit that extends between 10.5°S and 13.6°S from outer shelf to upper slope depths (Krissek et al. 1980). Preservation and burial within this deposit is due to high bulk sedimentation rates, which are favored by reduced bottom velocities in the poleward directed undercurrent (Suess et al. 1987). At greater water depths, increasing fluctuations in the velocity and direction of bottom currents result in lower sedimentation rates (Reimers and Suess 1983), winnowing, and the accumulation of phosphorite crusts and nodules (Reimers and Suess 1983; Glenn and Arthur 1988).

Sediment sampling and in situ flux measurements—Sediment samples were taken during the R/V *Meteor* cruise M77-1/2 in October–December 2008, using a video-guided multiple corer (MUC) and two benthic landers (Biogeochemical Observatories — BIGO and BIGO-T) along a latitudinal depth transect at 11°S (Fig. 1; Table 1). Bottom-water O_2 levels of $<$ 2 μmol L^{-1} extended from $\sim$ 50-m to $\sim$ 500-m water depth (Fig. 2), hitherto referred to as OMZ. During the time of sampling, the shallow shelf Sta. 543 and Sta. 568, at 78-m and 85-m water depth, respectively, also displayed bottom-water O_2 levels $<$ 2 μmol L^{-1}. However, these sites might experience periodic oxygenation events similar to those observed at a 94-m-deep site off Callao (Gutiérrez et al. 2008). As with increasing water depth oxygenation events can be assumed to occur more rarely, we henceforth refer to the core of the OMZ as the depth range between 250 down to its lower boundary at $\sim$ 500 m.

Sediment cores (inner diameter: 10 cm) retrieved by MUC were immediately transferred into a cold room that was kept at in situ temperature (4°C). Core processing was performed within 1–2 h upon retrieval. Two parallel cores were processed for all MUC stations. The overlying bottom water was sampled and filtered through 0.2-μm cellulose acetate (CA) syringe filters, and the remaining water was siphoned off and discarded. The first one of the two parallel cores was vertically sectioned within a glove bag under an argon atmosphere. The sediments were transferred to 50-mL centrifuge tubes preflushed with argon, and pore water was separated using a refrigerated centrifuge for 20 min at 4500 revolutions per minute

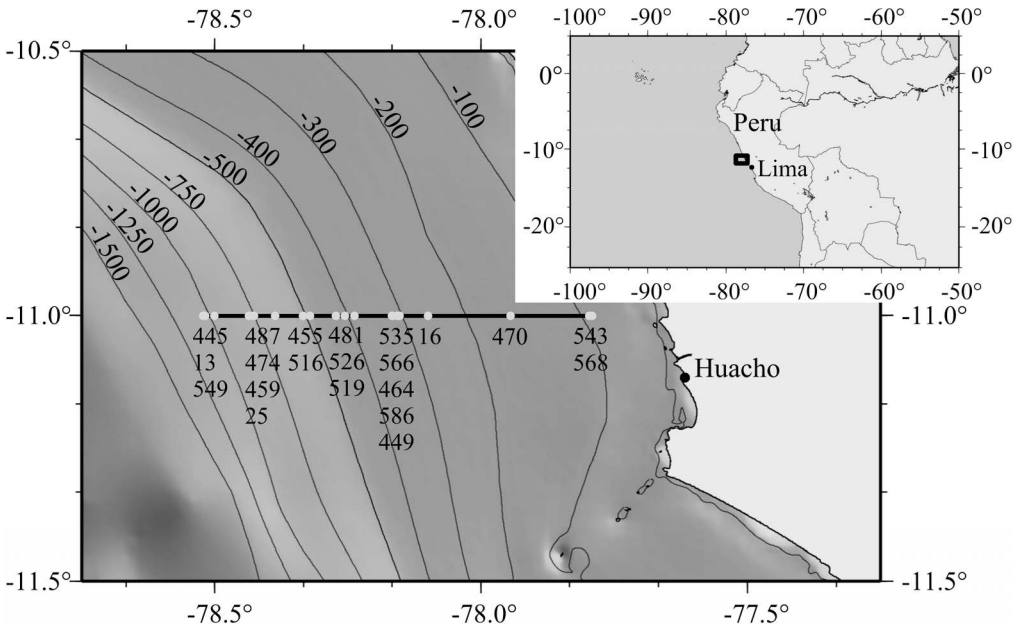

Fig. 1. Location map showing the Peruvian continental margin (bathymetry based on the Earth Topography Five Minute Grid [ETOPO5]). The sampling stations on the latitudinal transect at 11°S (horizontal line) are indicated by the gray dots. Where stations were close together, station names were listed in descending order in accordance with increasing water depth.

(rpm). Supernatant pore fluids were filtered under argon through 0.2-μm CA syringe filters. Centrifuge residuals were stored frozen for total sediment digestion and the extraction of highly reactive iron phases after the cruise. Pore water from the sediments retrieved at Sta. 543 and Sta. 516 was extracted using rhizons (Seeberg-Elverfeldt et al. 2005) instead of the glove bag method. Prior to deployment, the rhizons were preconditioned in an oxygen-free water bath. To ensure that the samples had not been in contact with air, the first 0.5 mL of extracted pore water were discarded. Pore waters from the other parallel core were extracted using a pore-water press (Teflon squeezers equipped with 0.2-μm CA filters), which was operated with argon at pressure gradually increasing to 2.5 bar. Additional samples for the determination of water content and porosity, as well as for total organic carbon (TOC) analyses, were taken from each depth interval, filled into preweighed plastic vials, and stored refrigerated for subsequent processing in the home laboratory. Squeeze cakes were also kept refrigerated until onshore preparation for x-ray fluorescence (XRF) analyses. Only the results from the glove bag extractions are presented in this study, if not otherwise indicated.

In situ benthic flux measurements were conducted using the biogeochemical observatories BIGO and BIGO-T (Sommer et al. 2009). BIGO contained two circular flux chambers (internal diameter 28.8 cm, area 651.4 cm^2). BIGO-T is similar to BIGO, but contained only one benthic chamber of the same size as those deployed in BIGO. An online video-controlled launching system allowed smooth placement of the observatories at selected sites on the seafloor. Two hours after the observatories were placed on the seafloor, the chamber(s) were slowly driven into the sediment ($\sim$ 30 cm h^{-1}). During this initial time period, the water inside the flux chamber was periodically replaced with ambient bottom water. After the chamber was fully driven into the sediment, the chamber water was again replaced with ambient bottom water to flush out solutes that might have been released from the sediment during chamber insertion. The water volume enclosed by the benthic chamber was in the range of 8.8 L to 18.5 L. To determine Fe^{2+} and TPO_4 fluxes, four sequential water samples were removed from the chamber with glass syringes (volume: $\sim$ 47 mL). The glass syringes were connected to the chamber using 1-m-long Vygon tubes with a dead volume of 6.9 mL. Prior to deployment, these tubes were filled with distilled water. In the case of the BIGO-T, the chamber was completely flushed with ambient seawater after half of the total deployment time, and a series of four water samples was taken before and after flushing, henceforth referred to as first incubation and second incubation, respectively. The flux measurements were conducted for different time periods in the range from 17.8 h to 23 h as defined from the time interval between the first and the last syringe water sampling. After recovery of the observatories, short cores (inner diameter: 10 cm) were retrieved from the incubated sediments and processed in the glove bag as described above for MUCs.

Chemical analyses—Onboard analytics: All shipboard analyses were performed shortly after pore-water extraction or recovery of benthic landers. Ammonium (NH_4^+), total dissolved sulfide (TH_2S), and total dissolved phosphate (TPO_4) analyses—in pore-water and incubated bottom-water samples—as well as dissolved ferrous iron (Fe^{2+}) analyses (in pore-water samples only) were realized onboard with a Hitachi U-2001 spectrophotometer, applying standard techniques (Grasshoff et al. 1999). Where

Table 1. Location, bottom-water oxygen concentration (BW O_2), and solid-phase geochemical data (TOC, TOC : P_{excess}, reactive Fe, and Fe : Al, each for 0–1 cm sediment depth) of the study sites during the R/V *Meteor* cruise M77/ 1-2. Further included are positions of CTD deployments for water column O_2 (representative profile shown in Fig. 2) and water column nutrients. Empty cells indicate that the parameter was not measured.

Station	Device	Cruise leg	Latitude (S)	Longitude (W)	Depth (m)	BW O_2 (μmol L^{-1})	TOC (wt%)	TOC : P_{excess}	Highly reactive Fe (wt%)	Fe : Al*
543	MUC 52	1	10°59.99′	77°47.40′	78	<2	3.50	181		0.46
568	BIGO 5	1	11°00.02′	77°47.72′	85	<2	3.76	297	0.36	0.44
470	MUC 29	1	11°00.02′	77°56.60′	145	<2	7.61	139	0.19	0.42
16	BIGO T	1	10°59.80′	78°05.91′	259	<2	13.54	171	0.12	0.41
535	BIGO T3	1	11°00.00′	78°09.12′	305	<2	15.18	140		
566	BIGO T4	1	11°00.00′	78°09.13′	309	<2	11.48			
464	BIGO 1	1	11°00.00′	78°09.92′	315	<2	15.45	134		
586	BIGO T5	1	11°00.00′	78°09.40′	316	<2	13.79	128		
449	MUC 19	1	11°00.01′	78°09.97′	319	<2	10.65	88	0.08	0.42
481	MUC 33	1	11°00.00′	78°14.19′	376	<2	10.86	58	0.09	0.38
526	BIGO 3	1	11°00.02′	78°15.27′	397	<2	14.75	95		
519	MUC 43	1	11°00.01′	78°16.29′	410	<2	8.50	43	0.07	0.36
455	MUC 21	1	11°00.00′	78°19.23′	466	<2	4.50	25	0.14	0.42
516	MUC 40	1	11°00.00′	78°20.00′	512	<2	6.07	3		0.42
487	MUC 39	1	11°00.02′	78°23.17′	579	4	6.48	26	0.12	0.37
474	BIGO 2	1	11°00.01′	78°25.55′	695	12	6.53	38		
459	MUC 25	1	11°00.03′	78°25.60′	697	12	6.72	53	0.32	0.48
25	BIGO	2	10°59.47′	78°26.10′	716	7	8.08	39		
445	MUC 15	1	11°00.00′	78°30.02′	928	39	5.15	20	0.26	0.87
13	BIGO	2	10°59.82′	78°31.05′	978	40	4.09	14		
549	MUC 53	1	10°59.81′	78°31.27′	1005	40	4.00	30	0.20	0.56
438	CTD-RO 16	1	11°00.69′	78°35.03′	1261					
463	CTD-RO 22	1	11°00.01′	78°44.86′	2031					

* From Scholz et al. 2011.

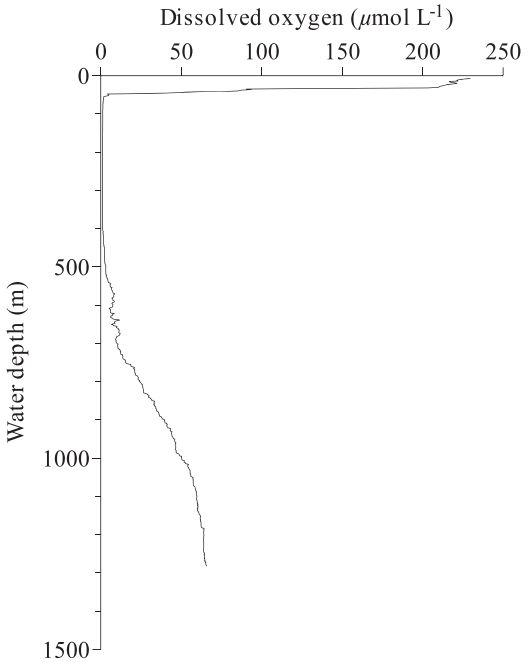

Fig. 2. Representative profile of dissolved oxygen (438 CTD-RO 16, position shown in Table 1) through the OMZ at 11°S during October–December 2008.

necessary, subsamples of pore water were diluted with oxygen-free artificial seawater prior to analysis. Ascorbic acid was added, still within the glove bag, to subsamples of pore and bottom waters for onboard Fe^{2+} analyses. Total alkalinity (TA) was determined by titration following the method of Ivanenkov and Lyakhin (1978). For selected cores, sulfate (SO_4^{2-}) was measured onboard by Ion Chromatography (716 IC-Compact, Metrohm). Sample aliquots for additional SO_4^{2-} analyses in the home laboratories were stored in plastic vials. Further information about the above-described analytical methods is available on the GEOMAR web site (www.geomar.de). For Fe analyses in the incubated bottom-water samples retrieved by benthic landers, aliquots were stored in acid-washed plastic vials and acidified with suprapure HNO_3. All sample aliquots were kept refrigerated until performance of analysis. Fe determinations were performed in the home laboratory by inductively coupled plasma mass spectrometry (ICP-MS Agilent 7500 series). Precision, determined by replicate analyses of calibration standards was $\leq 2\%$. We assume that all dissolved Fe released from the pore water is present as Fe^{2+}. Data on conductivity, temperature, depth (CTD) as well as oxygen bottom-water levels were taken from casts of a Sea-Bird Electronics, Inc., CTD system equipped with a water sampling rosette (RO), which were conducted nearby at each station investigated. During the CTD casts CTD-RO 16 and 22, water samples from Niskin bottles were spectrophotometrically analyzed for dissolved phosphate.

Solid phase analyses: Porosity was calculated from the weight loss of wet sediment during freeze-drying, assuming a dry solid density of 2 g cm^{-3} based on data published by Böning et al. (2004). Freeze-dried sediments were ground, pretreated with HCl to drive out carbonate carbon, and analyzed for TOC by flash combustion using a Carlo Erba Elemental Analyzer. Analytical precision for replicate samples was found to be 1%. The water content of centrifuge residuals was determined separately in order to recalculate the highly reactive Fe content for dry sediments.

Reactive Fe (term used in this article, which mainly combines Fe oxyhydroxides, Fe monosulfides (FeS), and Fe carbonates [Kostka and Luther 1994]) was extracted by adding 20 mL of cold 0.5 mol L^{-1} HCl to 0.5 g of wet sediment in 50-mL centrifuge tubes and shaking the samples for 1 h. The extracts were centrifuged, pipetted off, and filtered through 0.2-μm CA syringe filters. For total Fe determinations, 0.1-mL samples were added to 5 mL of a reducing ferrozine solution (1 g L^{-1} ferrozine in 50 mmol L^{-1} 4-(2-hydroxyethyl)-1-piperazineethanesulfonic acid [HEPES] buffer, pH 7, plus hydroxylammonium chloride [10 g L^{-1}]). After 20 min, Fe was measured at 562 nm using a Hitachi U-2001 spectrophotometer. Long-term precision of the in-house standard OMZ-1 was $< 5\%$ relative standard deviation.

Total concentrations of phosphorus and aluminum were analyzed by XRF spectrometry using a Philips PW 1480 spectrophotometer (equipped with a rhodium x-ray tube) on samples prepared as lithium tetraborate fused glass beads (ratio sample : flux 1 : 6). Loss on ignition was not determined for the samples, and P and Al contents were calculated from unnormalized oxides (P_2O_5, Al_2O_3). Average values of replicate analyses of different rock reference samples agreed well with the recommended values, and precision was better than 2% and 5% for P_2O_5 and Al_2O_3, respectively. Excess phosphorus (P_{excess}) was calculated as $P_{sample} - (P:Al_{andesite} \times Al_{sample})$ to remove the detrital P fraction according to Böning et al. (2004). The P : Al ratio for andesite was derived from Le Maitre (1976).

Flux calculations—Diffusive fluxes of Fe^{2+} and TPO_4 across the sediment–water interface (SWI) were calculated through application of Fick's first law of diffusion (Boudreau 1997).

$$J = -\Phi_0 D_s(dC/dz) \quad (1)$$

where Φ_0 is the porosity at the SWI (0–1 cm), D_s is the effective diffusion coefficient in the sediment at the SWI, and dC/dz is the pore-water gradient estimated from the concentration between the uppermost sediment interval (0–1 cm) and the bottom water. Bottom-water concentrations of TPO_4 were typically taken from measurements of Niskin bottle samples (463 CTD-RO 22, position shown in Table 1). In some cases, bottom-water concentrations of MUC samples seem to be artificially elevated because of sediment dispersal during sampling. However, the resulting difference in flux calculations is negligible. For each sampling site, molecular diffusion coefficients for ferrous iron (Fe^{2+}) and phosphate (HPO_4^-) in seawater corrected for in situ temperature (CTD measurements) were taken from Boudreau (1997) and further adjusted to in situ salinities and pressures by the Stokes Einstein relationship

(Li and Gregory 1974). The effective diffusion coefficient in the sediment was calculated from the adjusted molecular diffusion coefficient and tortuosity (derived by the empirical equation of Boudreau [1997]).

Solute concentrations obtained from the benthic chamber incubations were corrected for dilution with Milli-Q water originating from the water-filled Vygon tubing (V = 6.9 mL) connecting the individual syringes and the chamber. Benthic chamber fluxes were calculated from the slope determined by linear regression of the concentration versus the incubation time. During the deployments of BIGO 5 chamber 1 and 13 BIGO chamber 1 and chamber 2, the first data points were deviating from the subsequent ones. This might be due to a variety of reasons, such as contamination during subsampling onboard and laboratory handling, mixing of pore water into the enclosed water body when the benthic chamber was driven into the sediment, or failure of the water sampling system. In these cases, the first sample was excluded from the regression to calculate the respective fluxes. At the deeper, more-oxygenated stations below ~ 700-m water depth, it was not possible to measure a reliable flux of Fe^{2+} during the course of the benthic chamber incubations.

Results

Pore water—Pore-water profiles of Fe^{2+} and TPO_4 (from multicorer deployments) are shown in Fig. 3. Typically, distinct concentration maxima of Fe^{2+} were located close to the SWI in sediments overlain by the oxygen-depleted water body (< 2 μmol L^{-1}, Fig. 3). With increasing sediment depth, concentrations showed a strong decrease, and Fe^{2+} generally was no more detectable within 7 cm to 14 cm below the sediment surface. Highest concentrations of Fe^{2+} were measured in pore waters from the uppermost shelf station (543: 79.8 μmol L^{-1}, 1.5-cm depth) imposing a steep concentration gradient to the SWI. At stations underlying oxic bottom waters, the concentration peak shifted deeper into the sediment, and gradients between the uppermost sediment interval and the bottom water were very small or nonexistent. Similar to Fe^{2+}, highest TPO_4 concentrations typically occurred close to the sediment surface. Peaks generally shifted to greater sediment depth with increasing water depth. Except for the two shallowest stations, the concentrations decreased with increasing sediment depth below the maximum.

Profiles of some major pore-water constituents are exemplarily shown in Fig. 4 for three stations from the shallow shelf (Sta. 543), the OMZ core (Sta. 481), and below the OMZ (Sta. 549) to present trends across the transect and to provide the basis to relate TPO_4 and Fe^{2+} to the overall geochemistry of the setting (*see* General aspects of pore-water geochemistry). NH_4^+ and TA concentrations generally increased with sediment depth, reaching maximum values of 1.3 mmol L^{-1} and 13.7 meq L^{-1}, respectively, at shelf Sta. 543. Both NH_4^+ and TA markedly decreased with increasing water depth. SO_4^{2-} decreased only slightly with depth and at the shelf station, from 29.5 mmol L^{-1} to 23.5 mmol L^{-1} within 28-cm sediment depth, whereas no gradients were observed at the deeper stations. TH_2S was present only below 18 cm on the shelf, increasing to 760 μmol L^{-1} in the 26–30-cm interval; and it was undetectable over the sampled sediment length in the two other cores.

Benthic fluxes—The diffusive fluxes, as well as the chamber fluxes, of Fe^{2+} and TPO_4 are presented in Table 2 and illustrated in Figs. 5A and 6A, respectively, with positive fluxes being defined as from the sediment into the water column. The original data from the benthic chamber incubations can be provided from the authors on demand.

Total fluxes of dissolved Fe^{2+} and TPO_4 measured in benthic chambers were, in most cases, higher than the diffusive fluxes derived from pore-water gradients (Table 2). For sites located within the OMZ, ratios between fluxes measured by the chamber and diffusive fluxes average to 2.1 and 1.3 for Fe^{2+} and TPO_4, respectively. Limitations by depth resolution during pore-water sampling, leading to possible underestimation of the gradient's steepness, could have caused part of the discrepancy between the two methods. Furthermore, a significant fraction of the flux may have originated from the degradation of fresh organic matter (indicated by a thin fluffy layer covering numerous of the M77 cores) at the sediment–water interface that was not recorded in the pore-water profiles (Slomp et al. 1998). The contribution of biological pore-water irrigation to benthic chamber fluxes was probably negligible in the OMZ, due to its low significance in anoxic sediments, but may have been more important at the more-oxygenated stations. Consistently, diffusive phosphate fluxes displayed stronger deviations from chamber fluxes at deeper stations below the OMZ (range of ratios between chamber and diffusive fluxes: 3.3–8.6). On the shelf, benthic fluxes may have also been influenced by bioirrigation. Despite the strong oxygen deficiency, numerous small polychaetes were observed in sediment cores retrieved by the benthic chambers. This observation is in agreement with Levin et al. (2002) and Gutiérrez et al. (2008), who reported that bioturbating organisms rapidly invade the Peruvian shelf and upper slope during oxygenation events and may persist for several months after the recurrence of anoxic conditions.

Although these uncertainties are inherent to the pore-water–derived fluxes, these data reveal a spatial pattern across the transect similar to the benthic chamber fluxes. Hence the diffusive flux calculations provide reasonable approximations to total fluxes and can be used for a comparative study in the investigated area.

Solid phase data—Sediment geochemical data for reactive Fe, Fe : Al, TOC, and TOC : P_{excess} are provided in Table 1, Fig. 5 B,C (reactive Fe, Fe : Al), and Fig. 6 B,C (TOC, TOC : P_{excess}). Concentrations of reactive Fe were distinctively elevated at the shallow shelf stations, which are subjected to periodic oxygenation events (Gutiérrez et al. 2008), and below 600-m water depth, where O_2 levels increased (Fig. 5D). Concurrently with these increasing O_2 levels, Fe : Al ratios were above the average detrital background concentrations of 0.47 (Andean andesite;

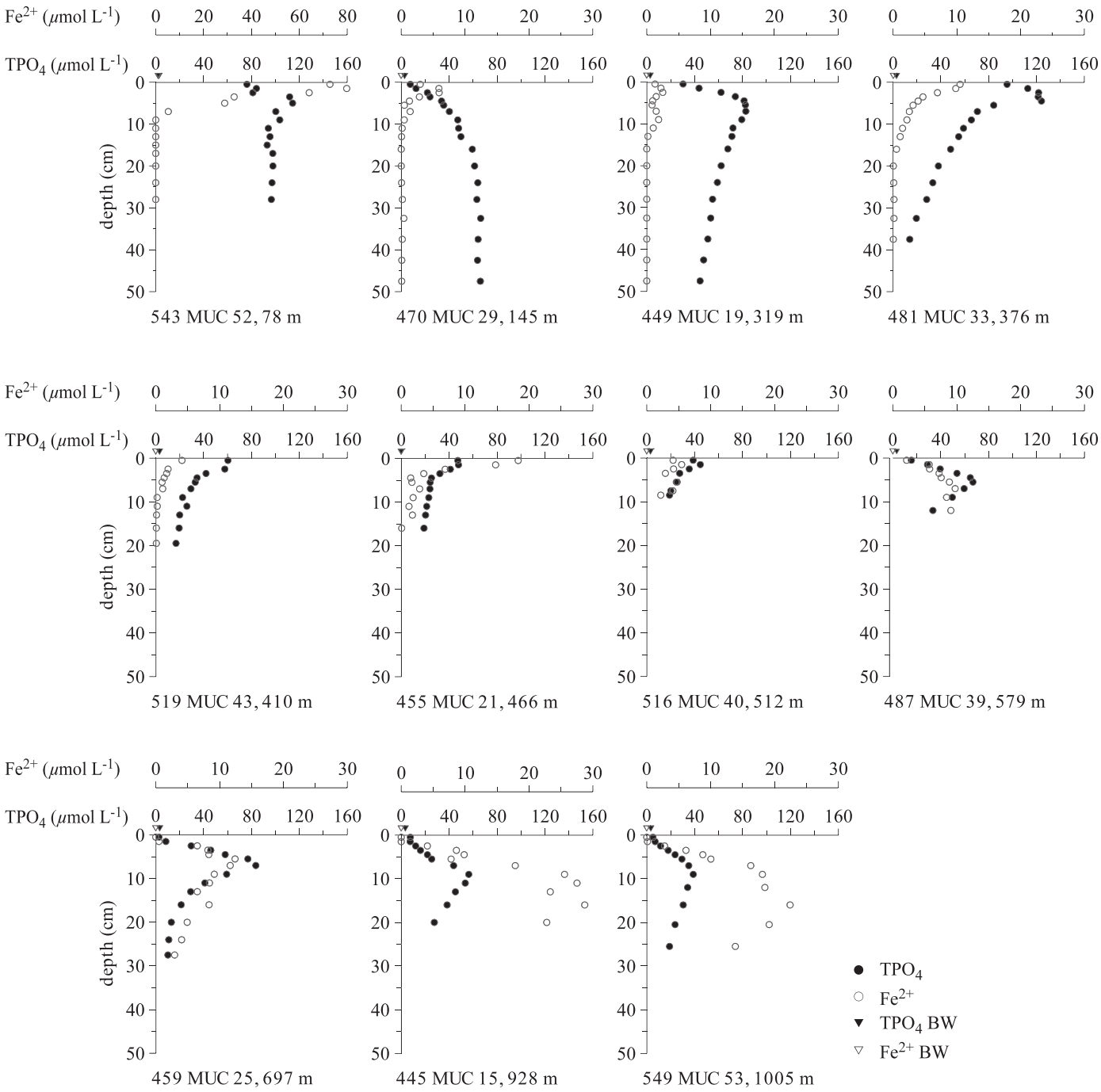

Fig. 3. Dissolved iron (Fe^{2+}, open circles) and phosphate (TPO_4, closed circles) pore-water profiles across the transect at 11°S. Sediments were retrieved using a multiple corer. Note: pore water at Sta. 543 and Sta. 516 was obtained by rhizon sampling. Triangles (open and closed for Fe^{2+} and TPO_4, respectively) indicate bottom-water concentrations, taken from CTD measurements for TPO_4.

Scholz et al. 2011). In contrast, at all shallower stations Fe : Al ratios were at and below the average (Fig. 5C). Measured TOC values were overall high, with a minimum concentration of 3.5 wt% on the shallow shelf and a maximum concentration of 15.5 wt% in the core of the OMZ (Fig. 6B). $TOC : P_{excess}$ ratios were elevated above Redfield ratio (106 : 1) at water depths ≤ 316 m; below 400 m, values were typically below 50 (Fig. 6C).

Discussion

General aspects of pore-water geochemistry—Peru margin sediments are characterized by significant organic matter degradation rates, which is demonstrated by the concurrent buildup of NH_4^+ and TA with sediment depth at all stations (Fig. 4). Pore-water gradients of NH_4^+ and TA reflect a decrease in organic matter degradation with

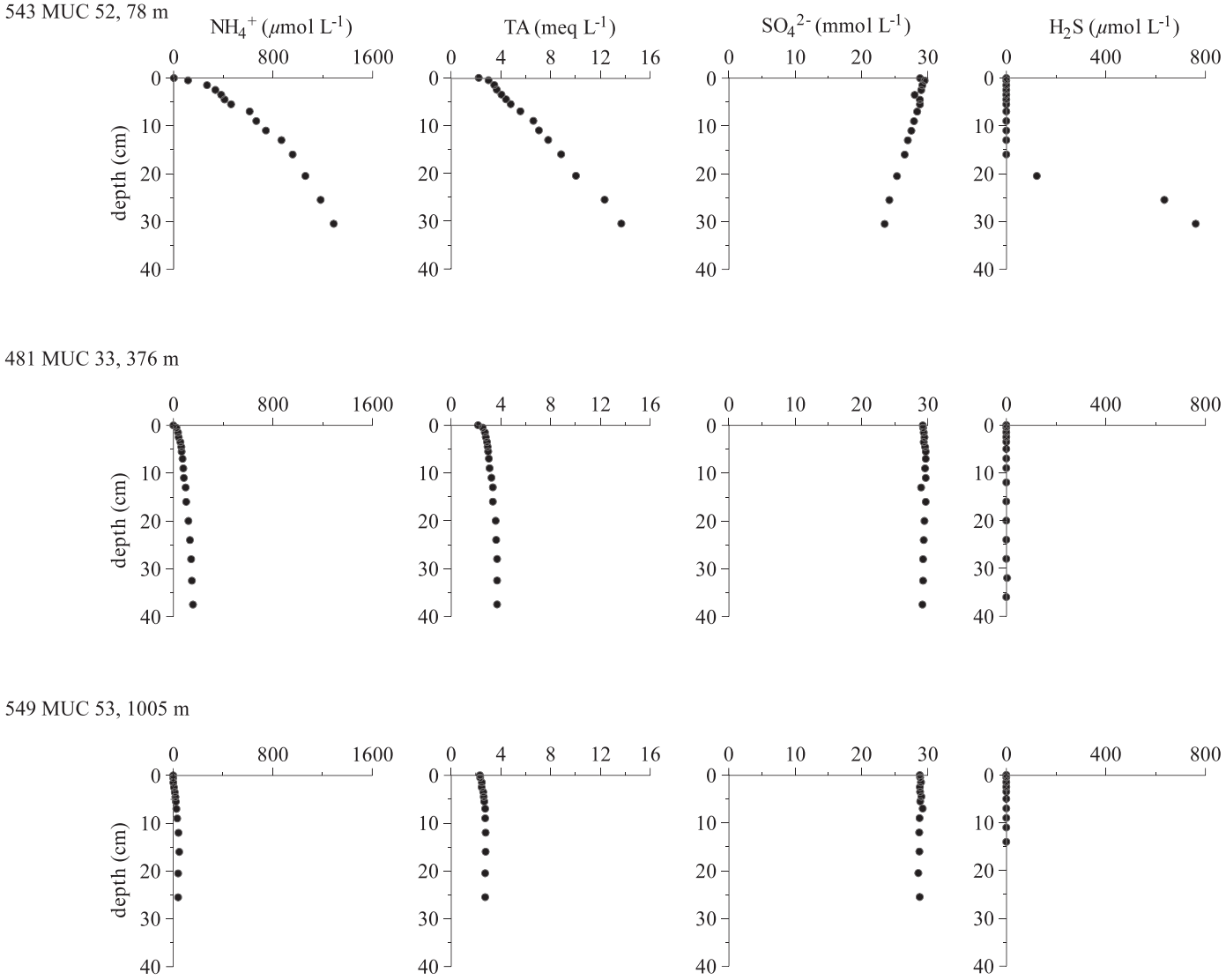

Fig. 4. Pore-water profiles of major pore-water constituents (NH_4^+, TA, SO_4^{2-}, and TH_2S) shown exemplarily for stations from the shallow shelf (Sta. 543), the OMZ core (Sta. 481), and below the OMZ (Sta. 549). The uppermost data point from each profile (depth of zero) represents the bottom-water concentration.

increasing water depth, which is generally consistent with the organic carbon oxidation rates of 8.2 mmol m^{-2} d^{-1} to 2.1 mmol m^{-2} d^{-1} derived from pore-water modeling that was conducted on selected stations from the same cruise (Bohlen et al. 2011). At the shelf (Sta. 543, Fig. 4), decreasing pore-water SO_4^{2-} concentrations and the presence of TH_2S below 20-cm sediment depth indicate intense sulfate reduction. In fact, pore-water modeling indicates that sulfate reduction at the shelf and upper slope contributes 80% to the entire organic carbon degradation (Bohlen et al. 2011). At the deeper stations (Sta. 481 and 549 in Fig. 4), no TH_2S was detected, which can be explained by complete precipitation of TH_2S as Fe sulfides or Fe^{2+} availability exceeding sulfide release from sulfate reduction. Under nearly anoxic conditions down to ~ 500-m water depth, reduction of Fe oxyhydroxides in the uppermost sediment horizon supports diffusion of Fe^{2+} into the bottom water (Table 2; Fig. 3). In this area near-surface TPO_4 and Fe^{2+} enrichments point towards P release during the reductive dissolution of Fe oxyhydroxides. However, only the pore-water profiles from sites at water depths > 400 m have mostly coincident concentration maxima indicative of the direct coupling of P and Fe cycles. Whereas, at shallower stations, maxima of both species are at slightly different vertical positions, suggesting other P sources and Fe precipitation (*see* Controls on benthic phosphate release). At the more-oxygenated stations below ~ 500-m water depth, the Fe diagenetic front is located deeper in the sediment. Here, pore-water profiles of Fe^{2+} indicate the precipitation of upward-diffusing Fe^{2+} into Fe oxyhydroxides within the thin oxic surface layer (Fig. 3). The concurrent decline of TPO_4 indicates that this TPO_4 is adsorbed or coprecipitated. Below the TPO_4 maxima, concentrations decrease to the base of the cores. Similar

Table 2. Chamber flux measurements and diffusive (pore-water–derived) fluxes of dissolved Fe^{2+} and TPO_4. Fluxes are given in mmol m^{-2} yr^{-1}. Averages are given for chamber fluxes and for diffusive fluxes from lander deployments with more than one sediment core recovered, where ± corresponds to the minimum and maximum fluxes; dashes indicate that at the station reliable chamber flux calculations were not possible because Fe^{2+} concentration changes with time did not exceed the analytical error. At the MUC stations chamber fluxes are not available because chambers were not deployed. Also included are flux ratios (chamber : diffusive) of Fe^{2+} and TPO_4, molar Fe : P pore-water concentration ratios (calculated for the Fe^{2+} peak position), and organic carbon oxidation rates (C_{ox}). C_{ox} was estimated by calculating HCO_3^- fluxes from TA gradients where bottom-water O_2 concentration was < 2 μmol L^{-1}, in order to provide for each diffusive TPO_4 flux an organic carbon oxidation rate (*see* text for further explanation).

Station	Device	Cruise leg	Depth (m)	Fe^{2+} flux chamber	Fe^{2+} flux diffusive	Ratio Fe^{2+} flux chamber : diffusive	TPO_4 flux chamber	TPO_4 flux diffusive	Ratio TPO_4 flux chamber : diffusive	Fe : TPO_4 pore water	C_{ox}
543	MUC 52	1	78		179.3			193.7		0.95	3274*
568	BIGO 5	1	85	316.1±33.6	88.3±0.9	3.6	169.9±15.9	75.8±10.2	2.2		2822±399
470	MUC 29	1	145		6.6			12.3		0.27	1220
16	BIGO T	1	259	—	18.9	—	211.4±4.3	148.3	1.4		3852
535	BIGO T3	1	305	3.8	6.8	0.56	209.2±14.2	151.1	1.4		888
566	BIGO T4	1	309	31.3	13.0	4	64.9±12.8	83.4	0.78		1244
464	BIGO 1	1	315	14.9	9.8±3.4	1.5	292.2±1.4	144.4±28.1	2		2634±729
586	BIGO T5	1	316	—	8.4	—	83.5±3.2	116.9	0.71		638
449	MUC 19	1	319		3.3			73.1		0.04	814
481	MUC 33	1	376		23.0			210.9		0.11	1374
526	BIGO 3	1	397	30±6.1	30.7	0.98	179.2±13.6	227.6	0.79		1442
519	MUC 43	1	410		8.5			123.1		0.07	518
455	MUC 21	1	466		31.9			79.9		0.39	216
516	MUC 40	1	512		7.8			69.7		0.12	425*
487	MUC 39	1	579		4.3			25.4		0.16	
474	BIGO 2	1	695	—	0.4± 0.4	—	20.5±6.1	2.9±1.2	7.1		
459	MUC 25	1	697		0.0			−1.0		0.16	
25	BIGO	2	716	—	0.0	—	18.2	5.5	3.3		
445	MUC 15	1	928		0.0			6.3		0.51	
13	BIGO	2	978	—	0.0	—	64.6±1.8	7.5	8.6		
549	MUC 53	1	1005		0.0			2.3		0.74	

* Obtained by pore-water squeezing.

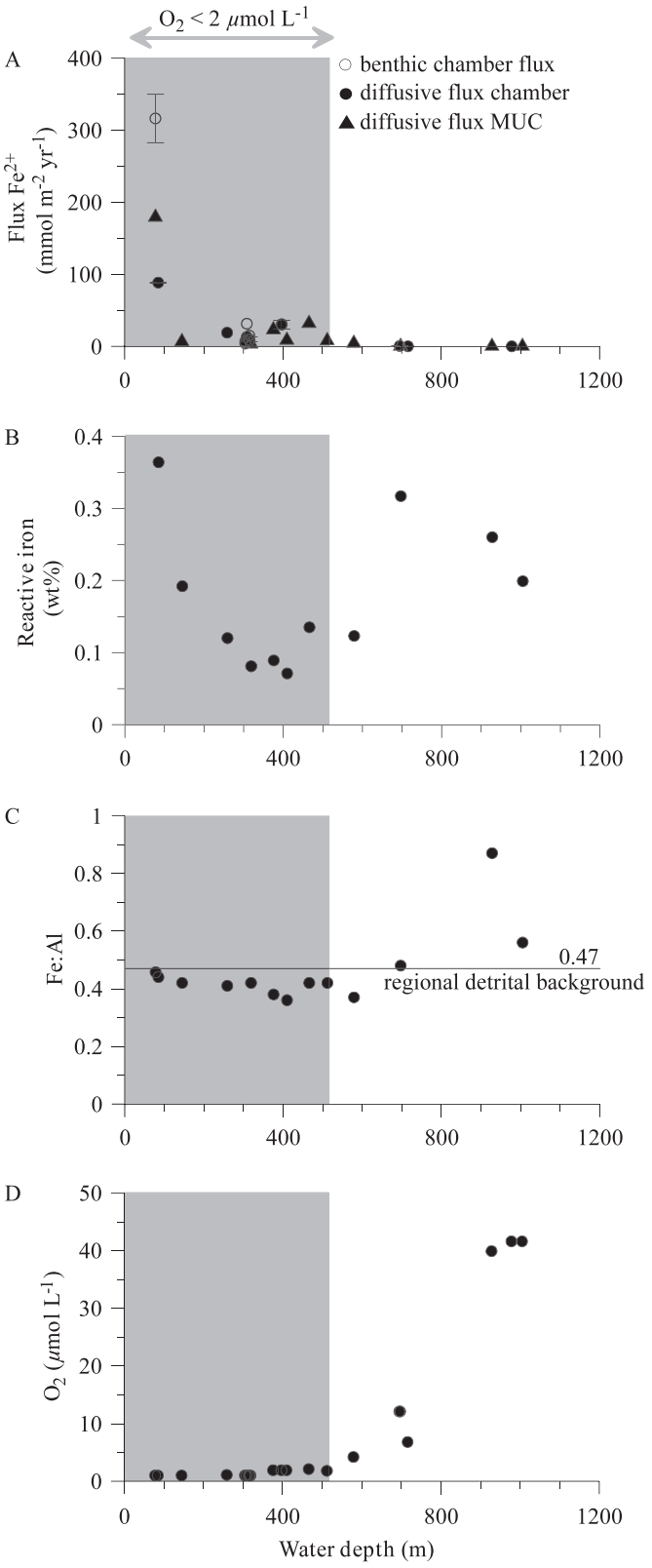

Fig. 5. Benthic Fe^{2+} fluxes and various parameters along the 11°S transect. (A) Fluxes of dissolved iron (Fe^{2+}; mmol m^{-2} yr^{-1}). Error bars correspond to minimum and maximum values of double measurements in lander deployments. (B) Reactive Fe contents (wt%) in surface sediments (0–1 cm). (C) Fe : Al ratios in surface sediments (0–1 cm; data from Scholz et al. 2011). Normalized Fe concentrations were used to eliminate the effect of varying dilution with detrital material. The black horizontal line depicts the Fe : Al ratio of the detrital background of 0.47 (andesite in the Andean Arc; Scholz et al. 2011). (D) Concentrations of dissolved O_2 in bottom waters. The gray array in each panel represents the OMZ where O_2 concentrations were < 2 µmol L^{-1}.

pore-water profiles of TPO_4 have previously been observed in the Peruvian (Froelich et al. 1988) as well as the Pakistan margin OMZ (Woulds et al. 2009) and have been attributed to carbonate fluorapatite precipitation.

Controls on benthic iron release—Dissolved Fe^{2+} fluxes across the sediment–water interface are controlled primarily by the bottom-water oxygen concentrations and the availability of reactive Fe (Pakhomova et al. 2007; Severmann et al. 2010). Under almost anoxic conditions (< 5 µmol O_2 L^{-1}; Table 1; Fig. 5D), elevated Fe^{2+} fluxes were observed down to ~ 600-m water depth. Below this depth, Fe^{2+} fluxes were negligible due to rising oxygen levels in the bottom water.

The highest Fe^{2+} fluxes measured on the shallow shelf at Sta. 543 and Sta. 568 (Table 2; Fig. 5A) coincide with the highest concentrations of reactive Fe (Fig. 5B), indicating high deposition rates of Fe oxyhydroxides. However, due to anoxic conditions right at the sediment surface, these become rapidly altered to Fe sulfides. Fe : Al ratios were close to the detrital background (Fig. 5C), which indicates that the reactive Fe is primarily supplied with Al and reflects a high input of detrital Fe oxyhydroxides from the continent. However, it is further plausible that part of the available Fe pool was deposited on the shelf during periods of bottom-water oxygenation, similar to those that were recorded during a long-term time series at a 94-m-deep site off Callao (Gutiérrez et al. 2008; M. Graco unpubl.). This time series revealed that, just prior to our research cruise, the shelf was oxygenated concurrent with a strong deepening of the oxycline (Fig. 7), reflecting the occurrence of a warming event along the Peruvian coast in association with Kelvin waves and the weakening of the coastal upwelling. During September 2008, the oceanographic conditions normalized and upwelling intensified. During such periods of shelf oxygenation, Fe^{2+} supplied from the deeper, permanent part of the OMZ may be reoxidized at the interface between anoxic and hypoxic water masses and be deposited on the seafloor. This mechanism has been suggested by Scholz et al. (2011), who showed that deposition and mobilization of trace metals on the Peruvian shelf is strongly affected by ENSO-related high amplitude oscillations of bottom-water oxygen concentrations (cf. Regional setting). During El Niño periods, surface sediments may also receive higher amounts of Fe oxyhydroxides from the continent because of heavy rainfall enhancing surface erosion and sediment discharge (Wells 1990). Dissolution of these Fe oxyhydroxides from either source induces increased Fe^{2+} fluxes when bottom-water conditions again turn anoxic, as was the case in September

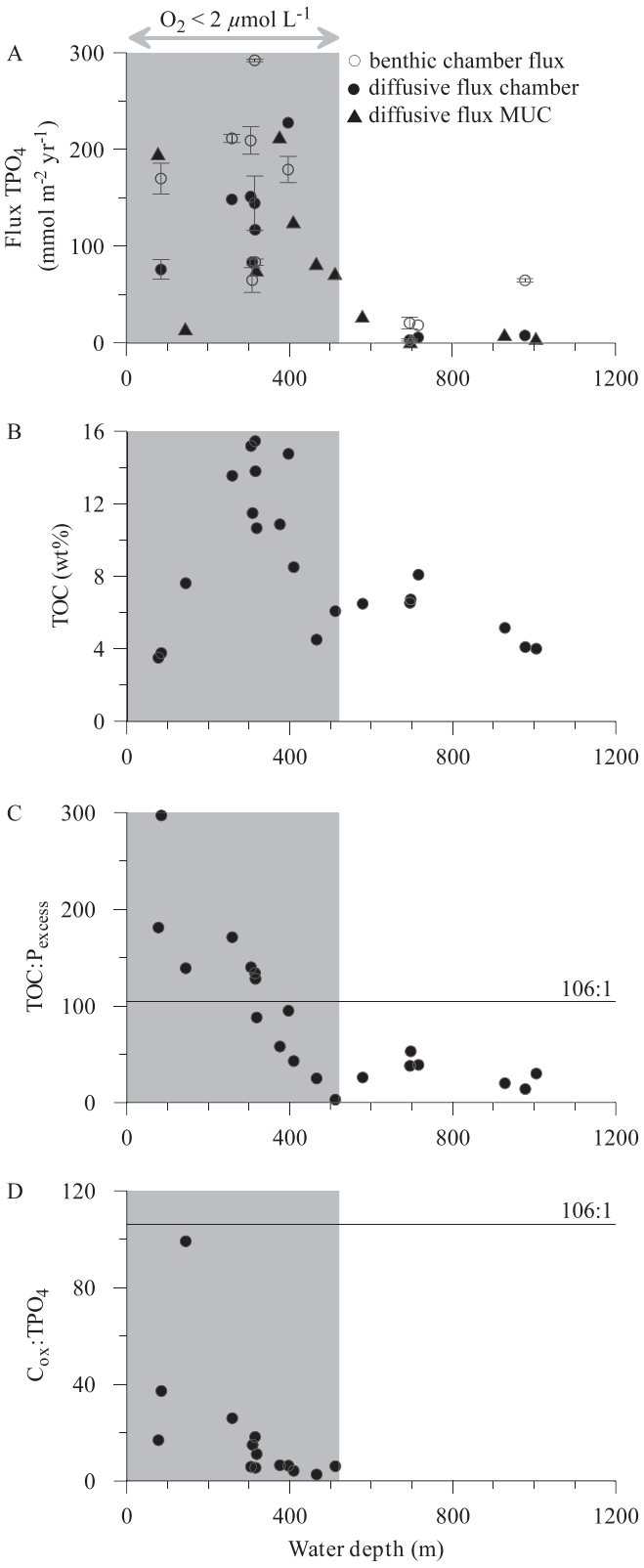

Fig. 6. Benthic TPO_4 fluxes and various parameters along the 11°S transect. (A) Fluxes of dissolved phosphate (TPO_4; mmol m^{-2} yr^{-1}). Error bars correspond to minimum and maximum values of double measurements in lander deployments. (B) TOC contents (wt%) in surface sediments (0–1 cm). (C) $TOC:P_{excess}$ ratios in surface sediments (0–1 cm). The black horizontal line depicts the TOC:P Redfield ratio of 106:1. (D) $C_{ox}:TPO_4$ flux ratios. The black horizontal line depicts the C:P Redfield ratio of 106:1. The gray array in each panel represents the OMZ where O_2 concentrations were < 2 µmol L^{-1}.

2008, about 1 month prior to the start of our research cruise at the end of October.

Intense sulfate reduction in the shelf sediments leads to the formation of Fe sulfides, which would be ultimately buried under permanently anoxic conditions. Under oxic bottom-water conditions, Fe sulfides may be recycled to the sediment surface by bioturbation and be reoxidized to Fe oxyhydroxides (Jørgensen and Nelson 2004). As mentioned in the Results section, there is a high potential for bioturbation at the shelf. However, the extent to which bioturbation affects the cycling of different Fe phases under oscillating oxic and anoxic bottom-water conditions and contributes to enhance overall Fe^{2+} flux on the shelf is not clear yet.

Within the core OMZ, Fe^{2+} fluxes were distinctly lower than at the 80-m stations, even though nearly anoxic bottom-water conditions (Table 1; Fig. 5A) provided suitable conditions for reductive Fe dissolution and release of Fe^{2+} across the benthic boundary. As oxygenation events can be assumed to occur more rarely down to these water depths, low bottom-water oxygen conditions in this region are supposed to be a persistent feature. Under such conditions, the reactive Fe pool will become progressively depleted over time. This is in agreement with the low reactive Fe concentrations as well as Fe:Al ratios significantly below the detrital background (Fig. 5B,C). Apparently, there is a strong imbalance between the reductive losses and the replenishment by detrital inputs from the continent in this region of the Peruvian margin.

Below about 700 m, increasing bottom-water oxygen concentrations (Table 1; Fig. 5D) cause the deepening of the redox front. Here, Fe^{2+} will be recycled within the sediment through reoxidation and reprecipitation in the surface layer (Fig. 3). Consequently, at these stations there was no flux of Fe^{2+} into the bottom water (Table 2; Fig. 5A). Both Fe:Al ratios and reactive Fe contents showed their maximum at ~ 900-m water depth (Fig. 5B,C) and showed decreasing values below. This strongly suggests that a large part of the Fe enrichment at the sediment surface derives from oxidative removal of Fe^{2+} that has been relocated from the core of the OMZ into the more-oxygenated deeper water layers. This is consistent with previous studies within the Arabian and Mexican OMZs that observed Fe enrichments linked to mechanisms of oxidative scavenging and OMZ relocation in sediments located below the OMZ (Van der Weijden et al. 1999; Nameroff et al. 2002).

Controls on benthic phosphate release—The distribution of TPO_4 fluxes along the transect (Fig. 6A) differs from that of Fe^{2+} (Fig. 5A), indicating different control mechanisms. While the release of Fe^{2+} from the seabed is largely

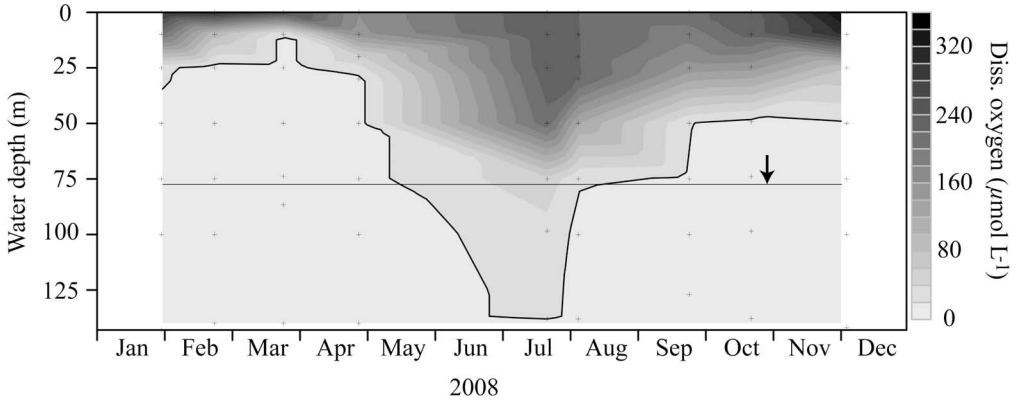

Fig. 7. Time-series of dissolved (diss.) oxygen (μmol L^{-1}) in 2008 off Callao (12°S). The gray horizontal line denotes the water depth of the shallowest station during the R/V *Meteor* cruise M77/1-2. The arrow denotes the start of this cruise. The black isoline corresponds to an oxygen concentration of 20 μmol L^{-1}.

determined by the availability of reactive iron that is reduced at the sediment surface, there are several sedimentary P sources that may contribute to the TPO_4 flux, comprising organic matter, iron bound P, and fish debris (Schenau and De Lange 2001).

With regard to P release driven by the reductive dissolution of Fe oxyhydroxides, the transect can be subdivided into distinct zones. At the sites shallower than 400-m water depth, noncoincident peaks of Fe^{2+} and TPO_4 indicate that TPO_4 liberation is at least partially decoupled from the reductive dissolution of Fe oxyhydroxides. In contrast, pore-water profiles of TPO_4 and Fe^{2+} from below 400-m water depth display similar trends, suggesting concurrent P release from the reductive dissolution of Fe oxyhydroxides. At all sites, the molar Fe : P ratios in the pore water at the peak position of Fe^{2+} ranged from 0.04 to 0.95 (Table 2), which is similar to Fe : P ratios measured in coastal sediments under anoxic conditions (Gunnars and Blomqvist 1997; Rozan et al. 2002; Lehtoranta and Heiskanen 2003). Such low Fe : P ratios indicate that, in addition to P release during reductive Fe dissolution, there was a further P source. If P release would be driven by the reductive Fe dissolution alone, one would expect Fe : P ratios in the range of 2 to 20 (Slomp et al. 1996; Gunnars and Blomqvist 1997; Anschutz et al. 1998). Another explanation for these low Fe : P ratios and the decoupling of pore-water TPO_4 and Fe^{2+} is the rapid formation of Fe sulfides (Rozan et al. 2002). For sites shallower than 400 m, sulfate reduction represents the major pathway of organic matter degradation (Bohlen et al. 2011), so that free dissolved Fe^{2+} can only exist in a narrow zone (< 10 cm) below the sediment surface.

At water depths between 250 m and 600 m (O_2 < 5 μmol L^{-1}), reactive Fe oxyhydroxides were almost absent (Fig. 5B); hence, Fe-bound P can obviously not serve as an important P source. At these sites, P release might be driven by organic matter degradation and dissolution of fish scales (*see* below). Only at the shallow shelf (Sta. 543), where the Fe : P ratio was close to unity, and at stations deeper than 600 m, Fe-bound P might be of some importance to the P cycle. On the shallow shelf, Fe oxyhydroxides are mainly supplied by the discharge of detrital sediments and reoxidation of dissolved Fe^{2+} when the shelf is oxygenated. Below 600-m water depth, Fe oxyhydroxides accumulate in the sediments, mainly due to the precipitation of dissolved Fe^{2+} at the lower oxycline (Scholz et al. 2011). However, at these stations both Fe and P are recycled within the sediment, resulting in low to zero fluxes.

In general, the deposition and degradation of organic matter in surface sediments underlying the OMZ is enhanced by enormous rates of surface-water productivity (Suess 1981). Consequently, organically bound P can be assumed as a major source contributing to the benthic TPO_4 flux. This is corroborated by the general agreement between TPO_4 fluxes (Fig. 6A) and the TOC content in surface sediments along the entire transect except the shallow shelf (Fig. 6B). Despite the lower TOC contents on the shelf, high organic carbon degradation rates of up to 8.2 mmol m^{-2} d^{-1} were calculated (Bohlen et al. 2011). Transient bottom-water oxygen levels are assumed to enhance organic matter degradation in sediments, leading to comparatively low TOC contents (Aller 1994). Another explanation is that at this site the solid phase composition is likely altered due to higher detrital sediment input. Below 600-m water depth, TPO_4 fluxes decreased distinctively despite still relatively high levels of TOC contents. This is due to increasing bottom-water O_2 levels and decreasing carbon degradation rates (Bohlen et al. 2011). Typically, high TOC : P ratios are observed in oxygen-deficient environments, indicating the preferential release of P over C (Ingall et al. 1993). The TOC : P_{excess} ratio shown in Fig. 6C is corrected for the detrital P fraction (Böning et al. 2004) and represents a measure for the total reactive P. Down to 300-m water depth, the TOC : P_{excess} ratios in surface sediments were distinctively elevated above the Redfield ratio, which is in agreement with TOC : P_{excess} ratios measured previously in the same area (Böning et al. 2004). At sites below 300-m water depth, the strong decrease of TOC : P_{excess} ratios may indicate the formation of authigenic P-bearing minerals and the accumulation of fish debris. Particularly, between 300-m and 400-m water depth, where high TPO_4 fluxes correspond to low TOC : P_{excess} ratios in the sediment, it is likely that P regeneration from organic matter is masked by the

formation of authigenic minerals. Phosphorus accumulation in the form of phosphorites is well known in the Peruvian OMZ (Glenn and Arthur 1988), and we also found numerous macroscopic phosphorite concretions in sediment cores retrieved from water depths between 300 m and 600 m.

In order to provide a first-order estimate on how the measured TPO_4 fluxes relate to available P sources in the sediment, we exemplarily calculated "theoretical" TPO_4 fluxes for the sites at 85-m and 309-m water depth that would result from organic matter degradation in surface sediments (assuming Redfield ratio) and Fe-bound P. TPO_4 fluxes related to the reduction of Fe oxyhydroxides (TPO_4–Fe) were calculated from benthic Fe^{2+} fluxes (Table 2) and the molar Fe : P ratio of Fe oxyhydroxides, which is typically about 10 (Slomp et al. 1996). P release from the breakdown of organic matter (TPO_4–C_{ox}) was derived by approximating organic carbon degradation (C_{ox}, Table 2) in surface sediments underneath a nearly anoxic water body ($O_2 < 2$ μmol L^{-1}) using TA pore-water gradients. C_{ox} can be calculated from TA gradients because HCO_3^- rather than CO_2 is produced in anoxic diagenetic pathways (Froelich et al. 1979). Under near-neutral conditions, HCO_3^- contributes more than 90% to TA, so that the TA gradient can be reasonably well applied to calculate a diffusive HCO_3^- flux and, hence, use it as a proxy for C_{ox}. In addition, the values presented in Table 2 are in good agreement with modeled values of C_{ox} (Bohlen et al. 2011). The combined average flux of TPO_4–C_{ox} and TPO_4–Fe at the shelf (78–85 m, $n = 2$) was 53.5 mmol m^{-2} yr^{-1} and in the core of the OMZ (305–319 m, $n = 5$) was 13.0 mmol m^{-2} yr^{-1}. We are aware that the P release calculated from the Fe^{2+} flux represents a minimum estimate because it does not account for Fe^{2+} that is precipitated as FeS. These fluxes are a factor of 3 and 12 lower than the measured fluxes, which is in agreement with low molar C_{ox} : TPO_4 ratios of benthic fluxes (Fig. 6D, calculated from C_{ox} and TPO_4, Table 2). These results highlight the preferential release of P over C with respect to the average composition of marine organic matter from OMZ sediments. At the 85-m station, some of the mismatch between theoretical and measured TPO_4 fluxes could be leveled out, if the Fe : P ratio of Fe oxyhydroxides was distinctively lower. However, at 309 m, and at similar sites with low Fe^{2+} but high TPO_4 fluxes, any change in the Fe : P ratio would not help to further resolve the mismatch.

Apart from the non-Redfield degradation of organic matter there are a few other processes that may explain the high TPO_4 fluxes. Fish scales are exceptionally abundant in sediments of the Peruvian OMZ (Suess 1981), hence their dissolution may represent an important source of pore-water TPO_4 (Suess 1981; Schenau and De Lange 2001). In addition, storage and release of P by microorganisms and protozoans under oscillating oxic and anoxic conditions has been supposed to contribute to the benthic TPO_4 flux (Sannigrahi and Ingall 2005). Sannigrahi and Ingall (2005) provided evidence for the accumulation of polyphosphates in oxic sediments, whereas in anoxic sediments polyphosphates were absent. This has been interpreted as release of P under anoxic conditions when these organisms degrade their intracellular polyphosphate storage that was built up under oxic conditions, to gain energy. Recently, transient uptake and release of P under oscillating redox conditions has been reported for the giant sulfide-oxidizing bacteria *Thiomargarita namibiensis* and members of the genus *Beggiatoa* (Schulz and Schulz 2005; Goldhammer et al. 2010; Brock and Schulz-Vogt 2011). Widespread occurrence of filamentous sulfur bacteria on the Peruvian shelf and upper slope was observed in sediment samples and in seafloor images acquired during the same cruise (T. Mosch unpubl.). In fact, sulfur bacteria of the genera *Beggiatoa* and *Thioploca* are very common in OMZ sediments of the Peruvian and Chilean continental shelf as well as in other OMZs worldwide (Gallardo 1977; Levin et al. 2002; Gutiérrez et al. 2008). Within the context of episodic oxygenation events that occur at the Peruvian shelf and upper slope (Gutiérrez et al. 2008), we suggest that *Beggiatoa* can probably enhance TPO_4 fluxes via the above-described P metabolism. Sulfur bacteria have been further suggested to be involved in the formation of apatite, which contributes to mitigate P release from the seabed (Schulz and Schulz 2005). During ^{33}P radiotracer experiments, Goldhammer et al. (2010) observed the greatest conversion rates of phosphate to apatite mediated by sulfur bacteria under anoxic conditions. Apatite formation is indicated by decreasing pore-water phosphate concentrations with sediment depth at all sites except for the shelf. Despite constant P concentrations with increasing sediment depth, apatite formation can also be assumed for the shelf since in the absence of precipitation P would accumulate in the pore water due to organic matter degradation and the associated P release. However, it can not be resolved if, and to what extent, release of P from microbes contributes to apatite formation.

In conclusion, the OMZ represents an important Fe^{2+} and TPO_4 source to the bottom water. The core of the OMZ ($\sim$ 250–500 m), with rather stable bottom-water O_2 levels close to anoxia, is characterized with persistent but comparatively low Fe^{2+} and high TPO_4 fluxes. This is in strong contrast to the shelf region, which is subjected to oscillating bottom-water O_2 conditions that trigger a complex biogeochemical reaction network of Fe, P, and S turnover, resulting in transient high Fe^{2+} and TPO_4 release under anoxia. This renders the shelf a sensitive region that provides limiting nutrients to the surface water, allowing extensive phytoplankton blooms to develop in the Peruvian upwelling system.

Global significance of benthic phosphorus and iron fluxes from OMZs—To evaluate the importance of TPO_4 and Fe^{2+} fluxes in the Peruvian OMZ from a more general perspective, we compiled a comparative data set from other coastal upwelling and OMZ regions (Fig. 8). Overall, TPO_4 fluxes measured in this study generally exceed those reported from other OMZs throughout the world. The global benthic TPO_4 flux from oxic shelf and slope sediments (> 20 μmol L^{-1} O_2) has recently been estimated as 75×10^{10} mol yr^{-1} for an area of 90×10^6 km^2 (Wallmann 2010), corresponding to an average TPO_4 flux of 8 mmol m^{-2} yr^{-1}. The average TPO_4 flux from the

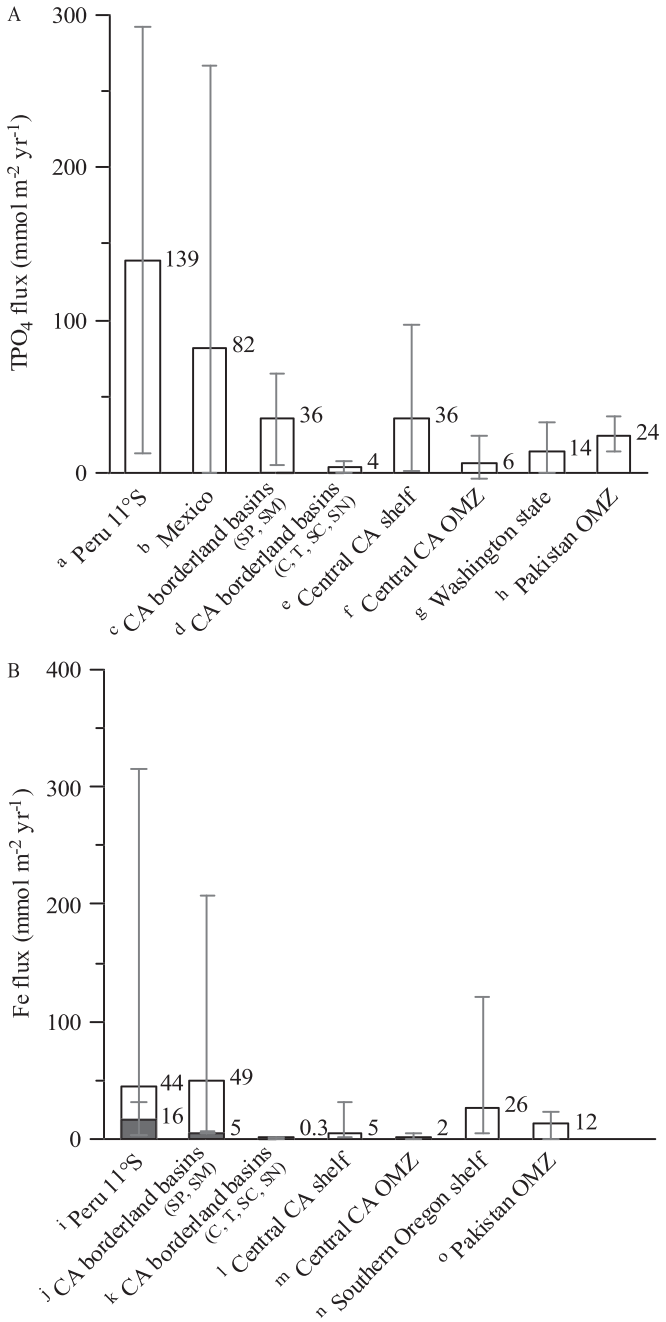

Fig. 8. Comparison of (A) phosphate (TPO_4) and (B) iron (Fe^{2+}) flux data from 11°S (total average of benthic chamber and diffusive fluxes for the OMZ ($O_2 < 2$ μmol L^{-1}, ~ 80–510-m water depth)) to data from other oxygen-deficient environments. Fluxes are given in mmol m^{-2} yr^{-1}. Values comprise single data points or total averages of all fluxes for any specific region. Fluxes shown by gray bars were calculated excluding high outlier Fe fluxes (*see* text for further explanation). (A) TPO_4 fluxes: [a]Peru 11°S; this study (water depth: 80–510 m, O_2: < 2 μmol L^{-1}), [b]Mexico; Hartnett and Devol 2003 (water depth: 100–1020 m, O_2: 0–6 μmol L^{-1}), [c]California borderland basins (SP = San Pedro basin, SM = Santa Monica basin); Berelson et al. 1987; Jahnke 1990; McManus et al. 1997; Hammond et al. 2004 (water depth: 900–910 m, O_2: 4–10 μmol L^{-1}), [d]California borderland basins (C = Catalina basin, T = Tanner basin, SC = San Clemente basin, SN = San Nicholas basin); Berelson et al. 1987; Bender et al. 1989; Ingall and Jahnke 1997; McManus et al. 1997; Hammond et al. 2004 (water depth: 1300–2070 m, O_2: 17–65 μmol L^{-1}), [e]Central California shelf; McManus et al. 1997; Berelson et al. 2003; Hammond et al. 2004 (water depth: 95–200 m, O_2: 64–185 μmol L^{-1}), [f]Central California OMZ; Reimers et al. 1992; McManus et al. 1997 (water depth: 530–1370 m, O_2: 16–65 μmol L^{-1}), [g]Washington State; Devol and Christensen 1993 (water depth: 40–630 m, O_2: 25–240 μmol L^{-1}), [h]Pakistan OMZ; Woulds et al. 2009 (water depth: 140–940 m, O_2: 1–3 μmol L^{-1}, post-monsoon). (B) Fe fluxes: [i]Peru 11°S; this study (water depth: 80–510 m, O_2: < 2 μmol L^{-1}), [j]California borderland basins (SP = San Pedro basin, SM = Santa Monica basin); McManus et al. 1997; Elrod et al. 2004; Severmann et al. 2010 (water depth: 880–910 m, O_2: 4–10 μmol L^{-1}), [k]California borderland basins (C = Catalina basin, T = Tanner basin, SC = San Clemente basin, SN = San Nicholas basin); McManus et al. 1997; Elrod et al. 2004 (water depth: 1300–2070 m, O_2: 17–65 μmol L^{-1}), [l]Central California shelf; McManus et al. 1997; Elrod et al. 2004; Severmann et al. 2010 (water depth: 95–200 m, O_2: 64–185 μmol L^{-1}), [m]Central California OMZ; McManus et al. 1997, Elrod et al. 2004 (water depth: 530–1370 m, O_2: 16–65 μmol L^{-1}), [n]Southern Oregon shelf; Severmann et al. 2010 (water depth: 90–190 m, O_2: 60–142 μmol L^{-1}), [o]Pakistan OMZ; Law et al. 2009 (water depth: 140–940 m, O_2: 1–3 μmol L^{-1}, post-monsoon).

Peruvian OMZ (< 2 μmol L^{-1} O_2) exceeds the average global flux from oxic shelf and slope environments by a factor of 17, which highlights the significance of anoxic sediments underlying the Peruvian and other OMZs as a major P source to the ocean.

Measurements of benthic Fe fluxes from continental shelf and slope sediments are only available from a very limited number of field studies. However, comparison with existing data reveals that fluxes presented in this study are among the highest recorded so far (Fig. 8). The highest total fluxes, associated with the highest variability, are observed on the shallow shelves, which typically experience the most intense environmental perturbations on various time scales. Including all stations of this study (Table 2), the resulting average flux in the Peruvian OMZ (< 2 μmol O_2 L^{-1}) is 44 mmol m^{-2} yr^{-1}, which is comparable to the average of 49 mmol m^{-2} yr^{-1} (white bars in Fig. 8) calculated for the California borderland basins (San Pedro and Santa Monica). Similar to the Peruvian shelf and upper slope, these basins are periodically ventilated (Berelson 1991), resulting in variable bottom-water oxygen concentrations and, hence, variable Fe fluxes (Severmann et al. 2010). The above average includes two high outlier fluxes (207 mmol m^{-2} yr^{-1}, San Pedro basin; 150 mmol m^{-2} yr^{-1}, Santa Monica basin; Severmann et al. 2010), measured when the basins were highly oxygen deficient (< 5 μmol O_2 L^{-1}). Fluxes measured when these sites were slightly more oxygenated (< 10 μmol O_2 L^{-1}, 5 mmol m^{-2} yr^{-1}) fall within the range of values measured in the Peruvian OMZ core at water depths > 85 m. Obviously, similar mechanisms of reoxidation during oxygenation periods and subsequent remobilization (resulting in highly elevated fluxes) during anoxic periods (*see* Controls on benthic iron release) are active in these settings. Exclusion of the highest

Fe fluxes measured at the Peruvian shelf stations (543, 568) and the outliers of the California borderland basins results in considerably lower average fluxes (gray bars in Fig. 8), which are comparable to those measured at river-dominated shelf sites (high reactive Fe input) from the Oregon and California margin (Severmann et al. 2010) or to those measured in the OMZ off Pakistan. Regardless of which data set is chosen, it is obvious that OMZs are major sources of dissolved Fe compared to normal marine environments. Based on an empirical relationship between Fe fluxes and organic carbon oxidation rates for settings > 20 μmol L^{-1} O_2, Elrod et al. (2004) estimated a dissolved Fe input of 8.9×10^{10} mol yr^{-1} for the global shelf area (3×10^7 km^2). This corresponds to an average Fe flux of 3 mmol m^{-2} yr^{-1}, which is obviously much lower than the average benthic Fe fluxes from sediments underlying oxygen-deficient waters and, hence, must be regarded as a minimum estimate.

An important pathway of Fe input to the surface ocean is atmospheric dust deposition. The following ''back-of-the-envelope'' calculation may illustrate how hotspots of benthic Fe mobilization compare to areas of high Fe input by dust deposition. One of the largest areas of atmospheric dust deposition is the tropical North Atlantic. Based on a composite map of dust delivery to the global oceans (Jickells et al. 2005), we calculated that the area of the North Atlantic hotspot (between 0–30°N) annually receives about 9.6×10^{10} kg dust, which translates into dissolved Fe fluxes of 3.4×10^7 kg yr^{-1} to 3.4×10^8 kg yr^{-1} that may become biologically available (assuming an Fe content of 3.5% in soil dust and an aerosol Fe solubility of 1–10% [Jickells and Spokes 2001]). Projecting the average Fe flux of 16–44 mmol m^{-2} yr^{-1} (Fig. 8) to a total area of the Peruvian OMZ ($O_2 < 0.5$ mL L^{-1} or 22 μmol L^{-1}) of 77,000 km^2 (Helly and Levin 2004) adds up to a total benthic flux of 6.9×10^7 kg yr^{-1} to 1.9×10^8 kg yr^{-1} and indicates that the source strengths of these completely different input mechanism are comparable in magnitude. However, at this time it is not clear if, and on which time scales, benthic Fe release may be considered as a potentially important source to the surface ocean. At least this could be significant in coastal upwelling systems with a low input of atmospheric dust, such as the Peruvian margin.

This study underlines the role of sediments underlying OMZs as important Fe^{2+} and TPO_4 sources to the bottom water, which provide important feedbacks that may affect surface-water primary productivity (Wallmann 2003) and, hence, accelerate the worldwide expansion of OMZs. Therefore, the investigation of benthic–pelagic coupling in oxygen-deficient waters along continental margins will require explicit consideration in the future.

Acknowledgments

We thank the captain and crew of the R/V *Meteor* for their effort and help during cruise M77/1-2, and A. Bleyer, B. Domeyer, M. Dibbern, R. Ebbinghaus, S. Kriwanek, D. Rau, and R. Surberg for help with biogeochemical analyses onboard and in the home laboratory. Furthermore, many thanks are due to B. Bannert, A. Petersen, and M. Türk for their technical assistance during benthic lander deployments; to P. Appel for management of XRF measurements; and, as well, to E. Piñero for her help with data treatment. We appreciate the editorial handling by Dr. Ronnie Glud and the constructive comments of three anonymous reviewers, which very much helped to improve the manuscript. This is a contribution of the Sonderforschungsbereich 754 ''Climate—Biogeochemistry in the tropical oceans,'' which is supported by the Deutsche Forschungsgemeinschaft.

References

Aller, R. C. 1994. Bioturbation and remineralization of sedimentary organic matter: effects of redox oscillation. Chem. Geol. **144:** 331–345, doi:10.1016/0009-2541(94)90062-0

Anschutz, P., S. Zhong, and B. Sundby. 1998. Burial efficiency of phosphorus and the geochemistry of iron in continental margin sediments. Limnol. Oceanogr. **43:** 53–64, doi:10.4319/lo.1998.43.1.0053

Bakun, A. 1985. Comparative studies and the recruitment problem: Searching for generalizations. CalCOFI Rep. **26:** 30–40.

Bender, M., R. Jahnke, R. Weiss, W. Martin, D. T. Heggie, J. Orchardo, and T. Sowers. 1989. Organic carbon oxidation and benthic nitrogen and silica dynamics in San Clemente Basin, a continental borderland site. Geochim. Cosmochim. Acta **53:** 685–697, doi:10.1016/0016-7037(89)90011-2

Berelson, W., and others. 2003. A time series of benthic flux measurements from Monterey Bay, CA. Cont. Shelf Res. **23:** 457–481, doi:10.1016/S0278-4343(03)00009-8

Berelson, W. M. 1991. The flushing of two deep-sea basins, southern California borderland. Limnol. Oceanogr. **36:** 1150–1166, doi:10.4319/lo.1991.36.6.1150

———, D. E. Hammond, and K. S. Johnson. 1987. Benthic fluxes and the cycling of biogenic silica and carbon in two southern California borderland basins. Geochim. Cosmochim. Acta **51:** 1354–1363, doi:10.1016/0016-7037(87)90320-6

Bohlen, L., and others. 2011. Benthic nitrogen cycling traversing the Peruvian oxygen minimum zone. Geochim. Cosmochim. Acta **75:** 6094–6111, doi:10.1016/j.gca.2011.08.010

Böning, P., H.-J. Brumsack, M. E. Böttcher, B. Schnetger, C. Kriete, J. Kallmeyer, and S. L. Borchers. 2004. Geochemistry of Peruvian near-surface sediments. Geochim. Cosmochim. Acta **68:** 4429–4451, doi:10.1016/j.gca.2004.04.027

Boudreau, B. P. 1997. Diagenetic models and their implementation. Springer.

Brock, J., and H. N. Schulz-Vogt. 2011. Sulfide induces phosphate release from polyphosphate in cultures of a marine *Beggiatoa* strain. ISME J. **5:** 497–506, doi:10.1038/ismej.2010.135

Devol, A. H., and J. P. Christensen. 1993. Benthic fluxes and nitrogen cycling in sediments of the continental margin of the eastern North Pacific. J. Mar. Res. **51:** 345–372, doi:10.1357/0022240933223765

Elrod, V. A., W. M. Berelson, K. H. Coale, and K. S. Johnson. 2004. The flux of iron from continental shelf sediments: A missing source for global budgets. Geophys. Res. Lett. **31:** L12307, doi:10.1029/2004GL020216

Froelich, P. N., G. P. Klinkhammer, M. L. Bender, N. A. Luedtke, G. R. Heath, D. Cullen, and P. Dauphin. 1979. Early oxidation of organic matter in pelagic sediments of the eastern equatorial Atlantic: Suboxic diagenesis. Geochim. Cosmochim. Acta **43:** 1075–1090, doi:10.1016/0016-7037(79)90095-4

———, and others. 1988. Early diagenesis of organic matter in Peru continental margin sediments: Phosphorite precipitation. Mar. Geol. **80:** 309–343, doi:10.1016/0025-3227(88)90095-3

Fuenzalida, R., W. Schneider, J. Garcés-Vargas, L. Bravo, and C. Lange. 2009. Vertical and horizontal extension of the oxygen minimum zone in the eastern South Pacific Ocean. Deep-Sea Res. II **56:** 992–1003, doi:10.1016/j.dsr2.2008.11.001

Gallardo, V. A. 1977. Large benthic microbial communities in sulfide biota under Peru-Chile subsurface countercurrent. Nature **268:** 331–332, doi:10.1038/268331a0

Glenn, C. R., and M. A. Arthur. 1988. Petrology and major element geochemistry of Peru margin phosphorites and associated diagenetic minerals: Authigenesis in modern organic-rich sediments. Mar. Geol. **80:** 231–267, doi:10.1016/0025-3227(88)90092-8

Goldhammer, T., V. Brüchert, T. G. Ferdelman, and M. Zabel. 2010. Microbial sequestration of phosphorus in anoxic upwelling sediments. Nat. Geosci. **3:** 557–561, doi:10.1038/ngeo913

Grasshoff, K., M. Erhardt, and K. Kremling. 1999. Methods of seawater analysis, 3rd ed. Wiley-VCH.

Gunnars, A., and S. Blomqvist. 1997. Phosphate exchange across the sediment-water interface when shifting from anoxic to oxic conditions—an experimental comparison of freshwater and brackish-marine systems. Biogeochemistry **37:** 203–226, doi:10.1023/A:1005744610602

Gutiérrez, D., E. Enríquez, S. Purca, L. Quipúzcoa, R. Marquina, G. Flores, and M. Graco. 2008. Oygenation episodes on the continental shelf of central Peru: Remote forcing and benthic ecosystem response. Prog. Oceanogr. **79**, 177–189, doi:10.1016/j.pocean.2008.10.025

Hammond, D. E., K. M. Cummins, J. McManus, W. M. Berelson, G. Smith, and F. Spagnoli. 2004. Methods for measuring benthic nutrient flux on the California margin: Comparing shipboard core incubations to in situ lander results. Limnol. Oceanogr.: Methods **2:** 146–159, doi:10.4319/lom.2004.2.146

Hartnett, H. E., and A. H. Devol. 2003. Role of a strong oxygen-deficient zone in the preservation and degradation of organic matter: A carbon budget for the continental margins of northwest Mexico and Washington State. Geochim. Cosmochim. Acta **67:** 247–264, doi:10.1016/S0016-7037(02)01076-1

Helly, J. J., and L. A. Levin. 2004. Global distribution of naturally occurring marine hypoxia on continental margins. Deep-Sea Res. I **51:** 1159–1168, doi:10.1016/j.dsr.2004.03.009

Hutchins, D. A., G. R. DiTullio, Y. Zhang, and K. W. Bruland. 1998. An iron limitation mosaic in the California upwelling regime. Limnol. Oceanogr. **43:** 1037–1045, doi:10.4319/lo.1998.43.6.1037

Ingall, E., and R. Jahnke. 1997. Influence of water column anoxia on the elemental fractionation of carbon and phosphorus during sediment diagenesis. Mar. Geol. **139:** 219–229, doi:10.1016/S0025-3227(96)00112-0

Ingall, E. D., R. M. Bustin, and P. Van Cappellen. 1993. Influence of water column anoxia on the burial and preservation of carbon and phosphorus in marine shales. Geochim. Cosmochim. Acta **57:** 303–316, doi:10.1016/0016-7037(93)90433-W

Ivanenkov, V. N., and Y. I. Lyakhin. 1978. Determination of total alkalinity in seawater, p. 110–114. *In* O. K. Bordovsky and V. N. Ivanenkov [eds.], Methods of hydrochemical investigations in the ocean. Nauka.

Jahnke, R. A. 1990. Early diagenesis and recycling of biogenic debris at the seafloor, Santa Monica Basin, California. J. Mar. Res. **48:** 413–436, doi:10.1357/002224090784988773

Jensen, H. S., P. B. Mortensen, F. Ø. Andersen, E. Rasmussen, and A. Jensen. 1995. Phosphorus cycling in a coastal marine sediment, Aarhus Bay, Denmark. Limnol. Oceanogr. **40:** 908–917, doi:10.4319/lo.1995.40.5.0908

Jickells, T. D., and L. J. Spokes. 2001. Atmospheric iron inputs to the oceans, p. 85–121. *In* D. R. Turner and K. A. Hunter [eds.], The biogeochemistry of iron in seawater. Wiley.

———, and others. 2005. Global iron connections between desert dust, ocean biogeochemistry, and climate. Science **308:** 67–71, doi:10.1126/science.1105959

Johnson, K. S., F. P. Chavez, and G. E. Friedrich. 1999. Continental shelf sediment as a primary source of iron for coastal phytoplankton. Nature **398:** 697–700, doi:10.1038/19511

Jørgensen, B. B., and D. C. Nelson. 2004. Sulfide oxidation in marine sediments: Geochemistry meets microbiology. Geol. Soc. Am. Spec. Pap. **379:** 63–81. doi:10.1130/0-8137-2379-5.63

Kostka, J. E., and G. W. Luther, III. 1994. Partitioning and speciation of solid phase iron in saltmarsh sediments. Geochim. Cosmochim. Acta **58:** 1701–1710, doi:10.1016/0016-7037(94)90531-2

Krissek, L. A., K. F. Scheidegger, and L. D. Kulm. 1980. Surface sediments of the Peru-Chile continental margin and the Nazca Plate. Geol. Soc. Am. Bull. **91:** 321–331, doi:10.1130/0016-7606(1980)91

Law, G. T. W., T. M. Shimmield, G. B. Shimmield, G. L. Cowie, E. R. Breuer, and S. M. Harvey. 2009. Manganese, iron and sulphur cycling on the Pakistan margin. Deep-Sea Res. II **56:** 305–323, doi:10.1016/j.dsr2.2008.06.011

Lehtoranta, J., and A.-S. Heiskanen. 2003. Dissolved iron : phosphate ratio as an indicator of phosphate release to oxic water of the inner and outer coastal Baltic Sea. Hydrobiologia **492:** 69–84, doi:10.1023/A:1024822013580

Le Maitre, R. W. 1976. The chemical variability of some common igneous rocks. J. Petrol. **17:** 589–637. doi:10.1093/petrology/17.4.589

Levin, L., and others. 2002. Benthic processes on the Peru margin: A transect across the oxygen minimum zone during the 1997–98 El Niño. Prog. Oceanogr. **53:** 1–27, doi:10.1016/S0079-6611(02)00022-8

Li, Y.-H., and S. Gregory. 1974. Diffusion of ions in sea water and in deep-sea sediment. Geochim. Cosmochim. Acta **38:** 703–714, doi:10.1016/0016-7037(74)90145-8

Matear, R. J., and A. C. Hirst. 2003. Long-term changes in dissolved oxygen concentrations in the ocean caused by protracted global warming. Glob. Biogeochem. Cycles **17:** 1125, doi:10.1029/2002GB001997

McManus, J., W. M. Berelson, K. H. Coale, K. S. Johnson, and T. E. Kilgore. 1997. Phosphorus regeneration in continental margin sediments. Geochim. Cosmochim. Acta **61:** 2891–2907, doi:10.1016/S0016-7037(97)00138-5

Moore, J. K., and O. Braucher. 2008. Sedimentary and mineral dust sources of dissolved iron to the world ocean. Biogeosciences **5:** 631–656, doi:10.5194/bg-5-631-2008

Nameroff, T. J., L. S. Balistrieri, and J. W. Murray. 2002. Suboxic trace metal geochemistry in the eastern tropical North Pacific. Geochim. Cosmochim. Acta **66:** 1139–1158, doi:10.1016/S0016-7037(01)00843-2

Pakhomova, S. V., P. O. J. Hall, M. Y. Kononets, A. G. Rozanov, A. Tengberg, and A. V. Vershinin. 2007. Fluxes of iron and manganese across the sediment-water interface under various redox conditions. Mar. Chem. **107:** 319–331, doi:10.1016/j.marchem.2007.06.001

Pennington, J. T., K. L. Mahoney, V. S. Kuwahara, D. D. Kolber, R. Calienes, and F. P. Chavez. 2006. Primary production in the eastern tropical Pacific: A review. Prog. Oceanogr. **69:** 285–317, doi:10.1016/j.pocean.2006.03.012

Reimers, C. E., R. A. Jahnke, and D. C. McCorkle. 1992. Carbon fluxes and burial rates over the continental slope and rise off central California with implications for the global carbon cycle. Glob. Biogeochem. Cycles **6:** 199–224, doi:10.1029/92GB00105

———, and E. Suess. 1983. Spatial and temporal patterns of organic matter accumulation on the Peru continental margin, p. 311–337. *In* J. Thiede and E. Suess [eds.], Coastal upwelling: Its sediment record. Part B: Sedimentary records of ancient coastal upwelling. Plenum Press.

Rozan, T. F., and others. 2002. Iron-sulfur-phosphorus cycling in the sediments of a shallow coastal bay: Implications for sediment nutrient release and benthic macroalgal blooms. Limnol. Oceanogr. **47:** 1346–1354, doi:10.4319/lo.2002.47.5.1346

Sannigrahi, P., and E. Ingall. 2005. Polyphosphates as a source of enhanced P fluxes in marine sediments overlain by anoxic water: Evidence from ^{31}P NMR. Geochem. Trans. **6:** 52–59, doi:10.1186/1467-4866-6-52

Schenau, S. J., and G. J. De Lange. 2001. Phosphorus regeneration vs. burial in sediments of the Arabian Sea. Mar. Chem. **75:** 201–217, doi:10.1016/S0304-4203(01)00037-8

Scholz, F., C. Hensen, A. Noffke, A. Rohde, V. Liebetrau, and K. Wallmann. 2011. Early diagenesis of redox-sensitive trace metals in the Peruvian upwelling area-response to ENSO-related oxygen fluctuations in the water column. Geochim. Cosmochim. Acta **75:** 7257–7276, doi:10.1016/j.gca.2011.08.007

Schulz, H. N., and H. D. Schulz. 2005. Large sulfur bacteria and the formation of phosphorite. Science **21:** 416–418, doi:10.1126/science.1103096

Seeberg-Elverfeldt, J., M. Schlüter, T. Feseker, and M. Kölling. 2005. Rhizon sampling of porewaters near the sediment-water interface of aquatic systems. Limnol. Oceanogr.: Methods **3:** 361–371, doi:10.4319/lom.2005.3.361

Severmann, S., J. McManus, W. M. Berelson, and D. E. Hammond. 2010. The continental shelf benthic iron flux and its isotope composition. Geochim. Cosmochim. Acta **74:** 3984–4004, doi:10.1016/j.gca.2010.04.022

Slomp, C. P., J. F. P. Malschaert, and W. Van Raaphorst. 1998. The role of adsorption in sediment-water exchange of phosphate in North Sea continental margin sediments. Limnol. Oceanogr. **43:** 832–846, doi:10.4319/lo.1998.43.5.0832

———, S. J. Van der Gaast, and W. Van Raaphorst. 1996. Phosphorus binding by poorly crystalline iron oxides in North Sea sediments. Mar. Chem. **52:** 55–73, doi:10.1016/0304-4203(95)00078-X

Sommer, S., and others. 2009. Seabed methane emissions and the habitat of frenulate tube worms on the Captain Arutyunov mud volcano (Gulf of Cadiz). Mar. Ecol. Prog. Ser. **382:** 69–86, doi:10.3354/meps07956

Stramma, L., G. C. Johnson, J. Sprintall, and V. Mohrholz. 2008. Expanding oxygen-minimum zones in the tropical oceans. Science **320:** 655–658, doi:10.1126/science.1153847

Strub, P. T., J. M. Mesías, V. Montecino, R. Rutland, and S. Salinas. 1998. Coastal ocean circulation of western South America, p. 273–313. *In* A. R. Robinson and K. H. Brink [eds.], The sea, v. 11. Wiley.

Suess, E. 1981. Phosphate regeneration from sediments of the Peru continental margin by dissolution of fish debris. Geochim. Cosmochim. Acta **45:** 577–588, doi:10.1016/0016-7037(81)90191-5

———, L. D. Kulm, and J. S. Killingley. 1987. Coastal upwelling and a history of organic rich mudstone deposition off Peru. *In* J. Brooks and A. J. Fleet [eds.], Marine petroleum source rocks. Geol. Soc. Spec. Publ. **26:** 181–197.

Sundby, B., L. G. Anderson, P. O. J. Hall, A. Iverfeldt, M. M. Rutgers van der Loeff, and S. F. G. Westerlund. 1986. The effect of oxygen on release and uptake of cobalt, manganese, iron and phosphate at the sediment-water interface. Geochim. Cosmochim. Acta **50:** 1281–1288, doi:10.1016/0016-7037(86)90411-4

———, C. Gobeil, N. Silverberg, and A. Mucci. 1992. The phosphorus cycle in coastal marine sediments. Limnol. Oceanogr. **37:** 1129–1145, doi:10.4319/lo.1992.37.6.1129

Van der Weijden, C. H., G. J. Reichart, and H. J. Visser. 1999. Enhanced preservation of organic matter in sediments deposited within the oxygen minimum zone in the northeastern Arabian Sea. Deep-Sea Res. I **46:** 807–830, doi:10.1016/S0967-0637(98)00093-4

Wallmann, K. 2003. Feedbacks between oceanic redox states and marine productivity: A model perspective focused on benthic phosphorus cycling. Glob. Biogeochem. Cycles **17:** 1084, doi:10.1029/2002GB001968

———. 2010. Phosphorus imbalance in the global ocean? Glob. Biogeochem. Cycles **24:** GB4030, doi:10.1029/2009GB003643

Wells, L. E. 1990. Holocene history of the El Niño phenomenon as recorded in flood sediments of northern coastal Peru. Geology **18:** 1134–1137, doi:10.1130/0091-7613(1990)018

Woulds, C., M. C. Schwartz, T. Brand, G. L. Cowie, G. Law, and S. R. Mowbray. 2009. Porewater nutrient concentrations and benthic nutrient fluxes across the Pakistan margin OMZ. Deep-Sea Res. II **56:** 333–346, doi:10.1016/j.dsr2.2008.05.034

Wyrtki, K. 1962. The oxygen minima in relation to ocean circulation. Deep-Sea Res. **9:** 11–23, doi:10-1016/0011-7471(62)90243-7

Associate editor: Ronnie Nøhr Glud

Received: 26 August 2011
Accepted: 29 January 2012
Amended: 27 February 2012